

SEISMIC MITIGATION EFFECT FOR LARGE-SPACE UNDERGROUND STRUCTURES CONSIDERING SPATIALLY VARYING SOIL PROPERTIES

Zhiming HE^{1,2}, Qingjun CHEN¹

¹*School of Civil Engineering, Tongji University, Shanghai, 200092, China*

²*School of Civil Engineering, Guangzhou University, Guangzhou, 510006, Guangdong Province, China*

Article History:

- received 7 June 2022
- accepted 31 May 2023

Abstract. The seismic response of the large-space underground structure (LSUS) is significantly influenced by the physical properties of the surrounding soil media, while the soil owns a strong spatial variability. This study proposes a seismic response analysis process of the soil-LSUS interaction system is proposed, which can consider the characteristic of the spatially distributed soil properties. The proposed process begins with establishing the spatially random field model of the soil properties using the improved latent space method. Then, the model is calibrated based on the real data and Bayesian approach, and the realization of the random field is accomplished. Further, the soil-LSUS interaction finite element (FE) model is established, which incorporating the soil physical properties generated from the random field. Finally, the nonlinear time-history analysis of the soil-LSUS interaction FE model is conducted. As an illustration of the proposed process, a typical LSUS located in Guangzhou is selected as an example, and the seismic mitigation measure which the lead-filled steel tube damper (LFSTD) is installed between the intermediate column and the top beam is adopted for the LSUS. The influence of the spatial variability of soil properties on the seismic mitigation effect of the LSUS is investigated. Results indicate that the spatial variability of the soil properties can cause a minor influence on the force and deformation of the intermediate column and the energy dissipation ratio between the LFSTD and structure, while it can bring a significant influence on the maximum deformation and force and the shape of the hysteresis loop of the LFSTD.

Keywords: underground structures, random fields, seismic response, soil-underground structure interaction.

 Corresponding author. E-mail: chiming@gzhu.edu.c

1. Introduction

Since the damage of underground structures during the 1995 Kobe earthquake has been widely reported, the safety of underground structures under earthquake impact has been re-evaluated, especially for the large-space underground structure (LSUS, e.g. underground subway stations, parking lots, and shopping malls) (Yamato et al., 1996; Tsinidis et al., 2020). At present, seismic failure mechanism of the LSUSs has been revealed, indicating that the intermediate column is the key component of the LSUS. Thus, to effectively resist the impact of strong earthquakes, different schemes have been proposed to upgrade the seismic performance of the LSUS (e.g., Ding et al., 2006; Yu et al., 2013, 2017; Do et al., 2015). Especially in the extension of the application of seismic isolation technology or energy dissipation devices, the effectiveness of installing seismic isolators (e.g., Ma et al., 2018) or dampers (e.g., Chen et al., 2014; He & Chen, 2021; Wang et al., 2021) within the cen-

tral column has been verified in reducing the structural seismic response.

Due to the factors such as the nature of the parent rock, erosion, transport process, and depositional conditions, physical properties of the soil are always various in spatial domain (Popescu, 1995; He et al., 2022). The characteristic of the strong spatial variability of soils can induce a certain influence on the mechanical behavior of the geotechnical system (Popescu et al., 2005). For instance, it can lead to the unsynchronized vibrations on the surface, and the inherent spatial variability of the shear strength of the soil can change its own bearing capacity failure mode (Popescu et al., 2005). Moreover, under the seismic loading, the coupling effect of the strong nonlinear characteristics of the soil and its own variability will further aggravate the variation of the soil, thereby affecting the dynamic response of the site furtherly (Popescu et al., 2005).

However, in the studies of the seismic mitigation scheme of LSUSs, soil properties are assumed to be layered and homogeneous along the horizontal direction, ignoring the spatial distribution distinction of soil properties. To have a more comprehensive understanding on the effectiveness of the proposed schemes, the influence of the spatial variability of the soil properties should be considered to further verify the seismic mitigation effectiveness of LSUSs. The geotechnical parameters own the spatial correlation and variability, while taking these parameters as random variables cannot fully reflect the spatial correlation between parameters. For this reason, random fields are usually used to capture the spatial distribution characteristics of the soil properties (e.g., Haldar & Babu, 2008; Na et al., 2009; Lizarraga & Lai, 2014; Zhang & Liu, 2020), and has been applied in dams (Hariri-Ardebili et al., 2019), slopes (Huang et al., 2017), and other engineering cases (He et al., 2022).

Along this line, an improved latent space method (ILSA) which considers the non-stationary characteristic of the random field is used to generate the spatially varying soil properties in this paper, and the random field models are updated by the Bayesian approach. On this basis, a seismic response analysis process of the soil-LSUS interaction system that can consider the spatially random distribution of soil properties is proposed. As an application of the proposed analysis process, a typical LSUS located in Guangzhou is selected to study the influence of the spatial variability of soil properties on the seismic mitigation effect of the LSUSs.

The rest of this paper is organized as follows. In Section 2, we introduce the whole process involving the simulation of the spatial random field of soil properties, including the proposed equations for modeling the spatial random field, Bayesian approach used in model calibration, and matrix decomposition method to realize the random field. Section 3 introduces the proposed seismic response analysis process of the soil-LSUS interaction system considering the random distribution of soil properties. The fourth section carries out the proposed framework into the modeling and seismic mitigation analysis of a representative LSUS. Section 5 summarizes the whole paper.

2. Random fields modelling the spatial distribution of soil properties

2.1. Random field formulation

When using random fields to simulate the spatial distribution of the soil properties, it is necessary to discretize the formation parameters, and generating a sample of the formation parameters at each position in space. In general, the spatial random field can be defined as the set of random variables in spatial domain under the condition considering the spatial correlation (VanMarcke, 1983; Xu & Gardoni, 2020). Following Xu and Gardoni (2018), a spatial random field is defined as

$$V(\mathbf{x}) = M(\mathbf{x}) + Z(\mathbf{x}) + \varepsilon(\mathbf{x}), \quad (1)$$

where $V(\mathbf{x})$ is the variable to be predicted in the random space, corresponding to this study, it represents the physical properties (e.g. unit weight, shear wave velocity, cohesion, and friction angle) of the soil that need to be simulated; $\mathbf{x} = [x_1, \dots, x_p]$ is the coordinates in random space, where p represents the dimensions of the random space which in general is 2 or 3; $M(\mathbf{x})$ is the mean-field; $Z(\mathbf{x})$ is a zero-mean, spatially correlated field; $\varepsilon(\mathbf{x})$ is the white noise that varies with space. For Eqn (1), the set of $V(\mathbf{x})$ is generally assumed to be a joint normal distribution. If the properties of the studied soil are non-normally distributed, Box-Cox transformation (Box & Cox, 1964) or iterative translation approach (Kim & Shields, 2015) can be used to achieve normalization.

In Eqn (1), the mean of $V(\mathbf{x})$ is $M(\mathbf{x})$, and its covariance is written as

$$\text{Cov}[V(\mathbf{x}), V(\mathbf{x}')] = \text{Cov}[Z(\mathbf{x}), Z(\mathbf{x}')] + \tau^2 I_{\mathbf{x}=\mathbf{x}'}, \quad (2)$$

where \mathbf{x} and \mathbf{x}' represent two different locations in random space; τ^2 is the variance of $\varepsilon(\mathbf{x})$; $I_{\mathbf{x}=\mathbf{x}'}$ represents the indicator function, which corresponds to 1 when $\mathbf{x} = \mathbf{x}'$ or 0 when $\mathbf{x} \neq \mathbf{x}'$.

In this study, to capture the non-stationarity characteristic of the random field, the Improved Latent Space Approach proposed by Xu and Gardoni (2018) is used to model the non-stationary covariance $\text{Cov}[V(\mathbf{x}), V(\mathbf{x}')]$,

$$\text{Cov}[Z(\mathbf{x}), Z(\mathbf{x}')] = \sigma[s(\mathbf{x})] \sigma[s(\mathbf{x}')] R(Q),$$

$$\text{where } Q = \sqrt{\begin{bmatrix} \mathbf{d}_{\mathbf{x}\mathbf{x}'} & \mathbf{d}_{\mathbf{s}\mathbf{s}'} \end{bmatrix} \begin{bmatrix} \boldsymbol{\theta}_{\mathbf{x}} & \mathbf{0}_{\mathbf{s}} \end{bmatrix}^{-1} \begin{bmatrix} \mathbf{d}_{\mathbf{x}\mathbf{x}'} & \mathbf{d}_{\mathbf{s}\mathbf{s}'} \end{bmatrix}^T}, \quad (3)$$

where $\sigma[s(\mathbf{x})]$ and $\sigma[s(\mathbf{x}')]$ represents the standard deviation of $Z(\mathbf{x})$ and $Z(\mathbf{x}')$, which are functions of the regressors at point \mathbf{x} and \mathbf{x}' ; $R(Q)$ is the stationary correlation function to the generalized distance Q ; $\mathbf{d}_{\mathbf{x}\mathbf{x}'} = [x_1 - x'_1, \dots, x_p - x'_p]$ is the Euclidean distance vector in the spatial dimension; $\mathbf{d}_{\mathbf{s}\mathbf{s}'} = [s_1 - s'_1, \dots, s_m - s'_m]$ is the distance vector of the regression variable in the latent space. $\boldsymbol{\theta}_{\mathbf{x}} = \text{diag}[\theta_{x_1}, \dots, \theta_{x_p}]$ is the scaling factor in the spatial dimension; $\mathbf{0}_{\mathbf{s}} = \text{diag}[\theta_{s_1}, \dots, \theta_{s_m}]$ is the diagonal matrix of high-order dimensional scaling factors.

2.2. Model calibration

A series of unknown parameters need to be estimated to establish the soil properties' random field model. When the corresponding data (i.e., the real soil property data that vary with space) is obtained, we estimate the unknown parameters involved in the random field model based on the Bayesian approach, achieving the calibration of the random field, which is written as

$$f(\boldsymbol{\theta}) = \gamma L(\boldsymbol{\theta}) p(\boldsymbol{\theta}), \quad (4)$$

where $f(\Theta)$ is the posterior distribution of Θ after being updated by the input data; γ is the normalization coefficient; $L(\Theta)$ is the likelihood function of the objective information contained of Θ in the input data; $p(\Theta)$ is the prior distribution about Θ . The posterior distribution of Θ is approximated by the Markov Chain Monte Carlo (MCMC) approach.

2.3. Realization of the spatial random field

We use the matrix decomposition approach to realize the spatially random field of soil properties (Davis, 1987; Xu & Gardoni, 2018). This method can deal with anisotropy problems in any correlation mode, and can reflect its anisotropy characteristics by establishing a correlation matrix (i.e., by selecting a suitable anisotropic correlation function and completing the assignment of the corresponding elements on the correlation matrix). Because of the simplicity of this approach, it has been widely used to simulate soil spatial variability (e.g., Kim & Santamarina, 2008; Wang et al., 2011; Papaioannou & Straub, 2012):

$$\mathbf{v} = \mathbf{m} + \mathbf{L}\mathbf{u}, \tag{5}$$

where \mathbf{v} represents one realization of the random field; \mathbf{m} represents the mean field obtained from $M(x)$ considering all spatial positions \mathbf{x} ; \mathbf{L} is the lower triangular matrix satisfying $\mathbf{L}\mathbf{L}^T = \mathbf{\Sigma}$, where $\mathbf{\Sigma}$ is the covariance matrix, and the

lower triangular matrix \mathbf{L} can be obtained by the Cholesky decomposition approach (Deodatis, 1996). \mathbf{u} is the realization of independent standard normal white noise.

3. Seismic response analysis process considering the spatial varying soil properties

3.1. FE model

After generating the random fields of soil properties, the following step is to establish the corresponding FE analysis model of the soil-LSUS interaction system, and the specific modeling process is shown in Figure 1. It has been demonstrated that the seismic response and damage of LSUSs are mainly controlled by the lateral deformation of the soil layer [1–4]. Therefore, this study only considers the variability in the horizontal and vertical directions.

The process begins with obtaining the design information of site and structure (e.g., drilling data, size of structural components, material type) according to the engineering project. Then, the calculation domain of the site and the coordinate system of the spatial random field are determined. Next, the size and element type of the soil unit is determined, and the size of the unit will affect the number of data points of the random field. Subsequently, the spatial random field of different soil properties is real-

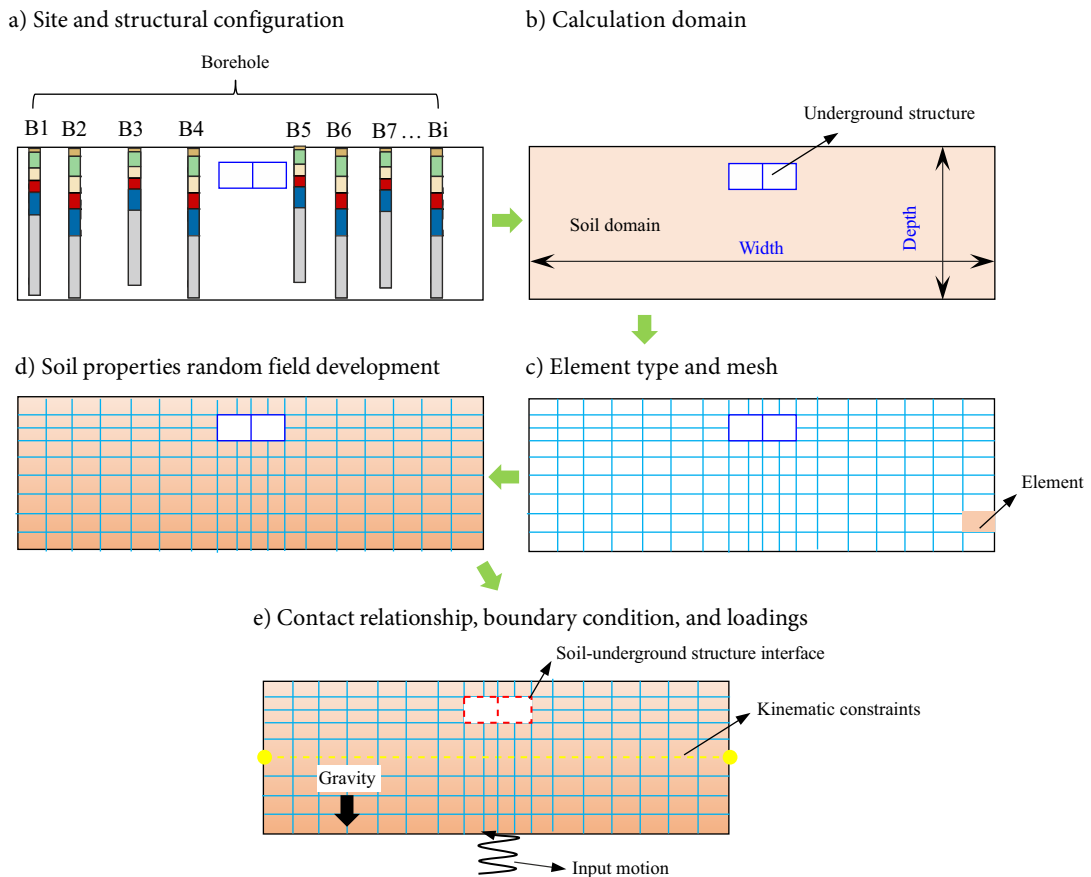


Figure 1. Flow chart of FE model development

ized following Section 1 and embed it into the FE model of the soil-LSUS interaction system. The last step is to define the properties of the dampers, contact properties between the soil and the structure, boundary conditions, and apply the whole loadings to the interaction system.

3.2. FE analysis process

The main steps of embedding the random field into the numerical model and conducting the analysis are as follows (as shown in Figure 2). Step 1, based on the general FEA software ABAQUS, the FE model of the soil-LSUS interaction system is developed following Section 2.1, and the model is exported as a "S-LSUS*.inp" file, which can be modified through a text editor. Step 2, the corresponding random fields are generated based on the approach introduced in Section 2, then, the data of the spatial distribution of soil properties are extracted according to the size of the element mesh, and are attributed to the soil unit of the FE analysis model. Step 3, using the Python tools, the material properties of each element in the "S-LSUS*.inp" file of step 1 are replaced with the properties generated in the random field in step 2, and then the non-linear time-history analysis of the soil-LSUS interaction system is conducted to obtain the structural seismic response. The last step, repeat steps 2 and 3, N times of time-history analysis are performed, and the analyses results such as the structural force and deformation are obtained.

4. Case study: modeling and seismic mitigation analysis of a typical LSUS

We perform the proposed seismic response analysis process in Section 3 with an example of a typical LSUS. A seismic mitigation scheme, which the Lead-filled Steel Tube Damper (LFSTD, i.e., a kind of metallic damper consisting of the steel tube, lead core, extrusion head, and connecting end plate, see Figure 3a installed between the intermediate column and the top beam (as shown in Figure 4) is used in this case, and the effectiveness of this scheme has been verified (He & Chen, 2021). The LFSTD can absorb the seismic energy through the relative deformation of the upper and lower end plates (see Figure 3b), to reduce the external input energy subject to the structure.

In this section, we first introduce the general information about the engineering design of this case, including details about the structure and the located site. Subsequently, in accordance with Section 1, the improved latent space approach is adopted to develop the spatial random field model of soil properties. Then, the developed model is calibrated using the measured borehole data through Bayesian approach, and the spatial distribution of the soil properties is obtained. Finally, a soil-LSUS interaction analysis model with installing the LFSTDs is established, which considering the spatial random distribution of soil properties, and the seismic response analyses are carried out in accordance with Section 2.

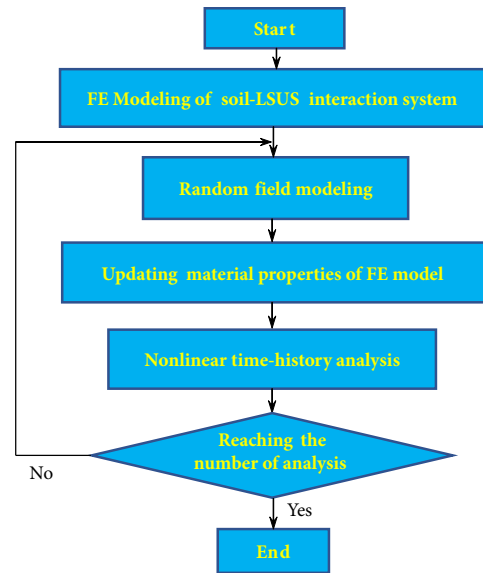
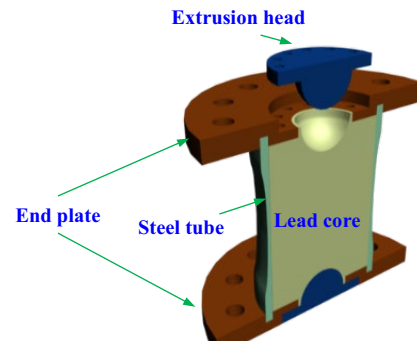


Figure 2. FE analysis process

a) Configuration profile



b) Deformation mode

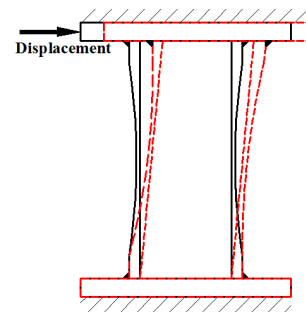


Figure 3. Introduction of the LFSTD

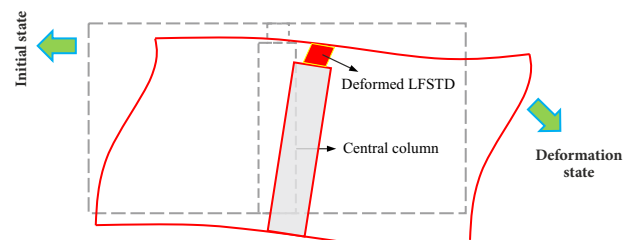


Figure 4. Working mechanism of the seismic mitigation scheme of the LSUS using LFSTDs

4.1. Soil and structural information

A typical LSUS located in Guangzhou is selected, and the plan of the research area is shown in Figure 5. The red line indicates the location of the drill hole of the project, and all the boreholes are aligned almost in a straight line. Figure 5 also shows the location of the structure (i.e., the light green shaded area) and direction of the structure (i.e., the orange line). Figure 6 depicts the stratum composition of each borehole, where the X- and Y- axes represent the relative position (along the red line) and depth of each borehole. The stratum contains soil types includes the cohesive backfill, silty clay, sandstone, argillaceous siltstone, and fine sand. We can find that the thickness of various soil layers is different, indicating an obvious spatial variability on the stratum.

It has been revealed that the stratum parameters such as the shear wave velocity, Poisson’s ratio, and gravity can cause a obvious influence on the seismic response of the LSUS (Huang et al., 2015). Figure 7 depicts the distribution of the physical properties of all boreholes along the depth, and the physical properties of each soil layer show significant differences along the depth. Based on the stratum information of each borehole, the studied site can be classified as Category II according to the Chinese Code for Seismic Design of Buildings (GB 50011-2010) (Ministry

of Housing and Urban-Rural Development of the People’s Republic of China, 2010), or correspondingly equivalent to Category C site following FEMA 356 (Federal Emergency Management Agency, 2000), Zhang and Liu (2020) and Category B following the European seismic code EC8 (European Committee for Standardization, 2005). The drilling depth of the boreholes (i.e., 32 to 36 m) meets the requirements for the survey of seismic engineering geological conditions (i.e., the selected sites are lying on the stiff soil with shear wave velocity greater than 500 m/s based on the local Code for Evaluation of Seismic Safety of Engineering Sites (GB 17741-2005) (National Standardization Management Committee, 2005).

Figure 8 depicts the cross-section of the studied LSUS, which is a typical rectangular box structure, with the buried depth of 4.0 m, the width of 37.4 m, and the height of 5.45 m. The thickness of the top and bottom plate of the structure are 0.6 m and 0.85 m, and the reinforcement ratio are both 1.0%. The thickness of the lateral walls is both 0.7 m, with the reinforcement ratio of 0.8%. The height of the central column is 3.6 m, with a cross-sectional dimension of 0.7 m×0.7 m, and the longitudinal spacing is 6.0 m and the reinforcement ratio is 5.6%. The concrete material adopts C40 strength grade (i.e., the standard compressive strength is 40 MPa), and the steel bar adopts HRB335 strength grade (i.e., the yield strength is 335 MPa).

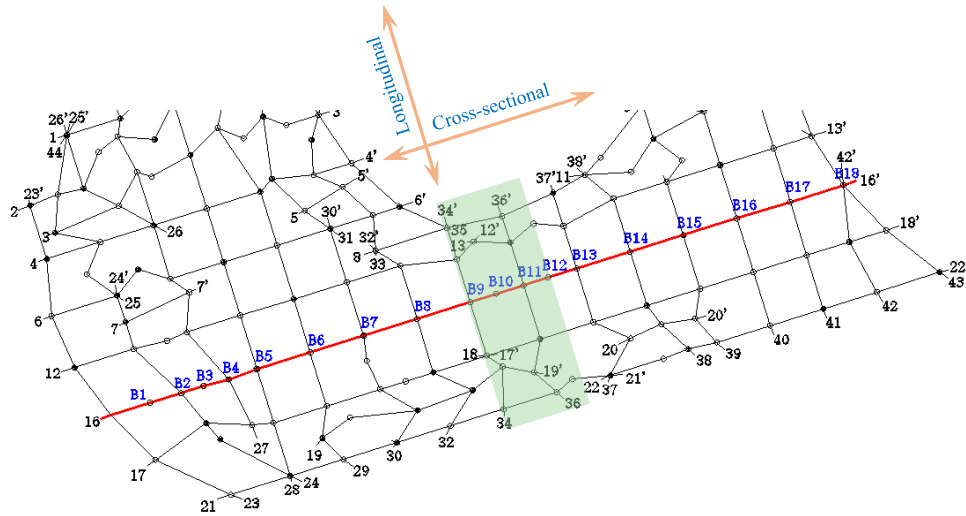


Figure 5. Plane of the study area

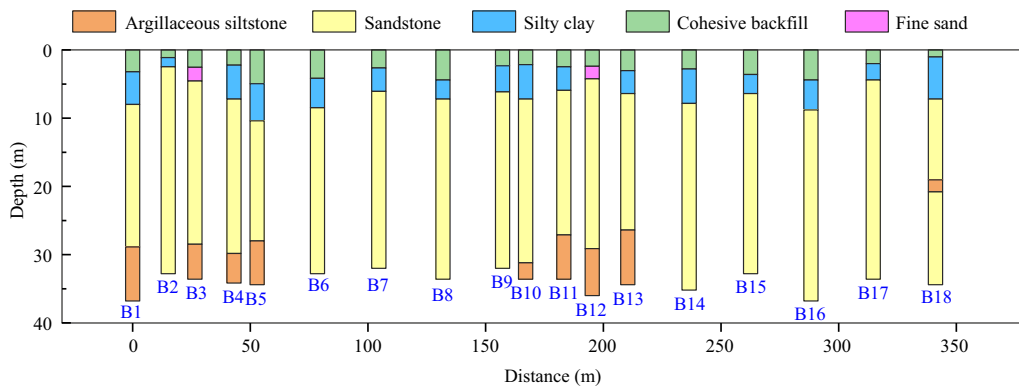


Figure 6. Relative distance and layer compositions of each borehole

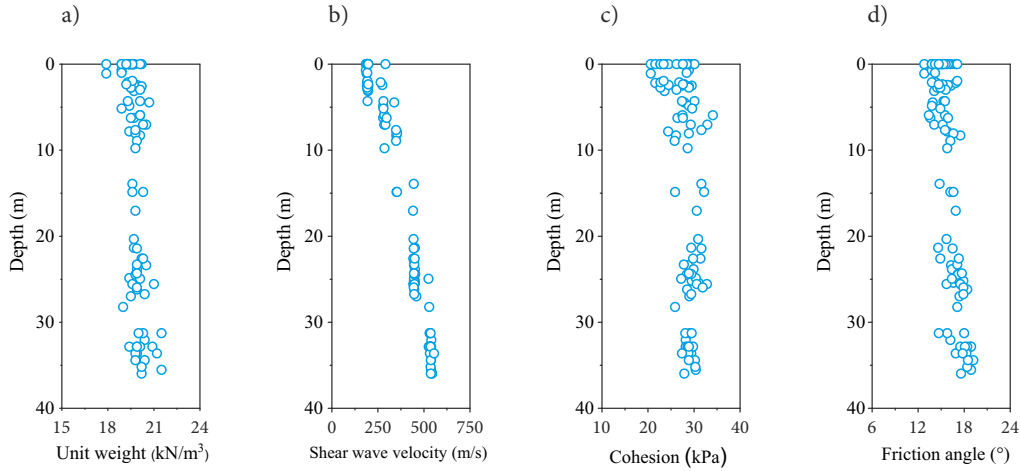


Figure 7. Distribution of physical properties of soil layers along the depth

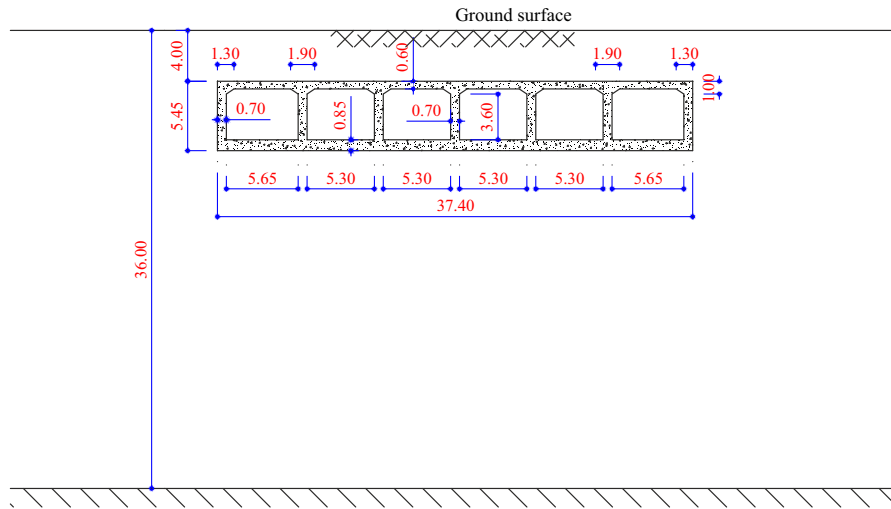


Figure 8. Cross-section of the studied LSUS. (unit: m)

4.2. FE model

According to the FE model developing process established in Section 2, we develop a three-dimensional soil-LSUS interaction analysis model based on the FE analysis platform ABAQUS, as shown in Figure 9. For step 2 in Section 2.1, we determine the depth of the soil domain in the FE model based on the deepest borehole (i.e., 36 m) obtained from the engineering site data (i.e., the engineering bedrock surface). For the consideration of lateral boundary conditions, we ignore the scattered and reflected effect on the seismic response of the soil-LSUS interaction system. To lower the analytical error caused by the wave reflection on the artificial boundary, we use 10 times the depth of the engineering bedrock as the width of the FE model following He and Chen (2021) and Wang et al. (2017) (i.e., the width is taken as 360 m). For the mesh of soil in FE model, the maximum size of the vertical grid h_{\max} is determined following Lysmer and Kuhlemeyer (1969), as

$$h_{\max} \leq \frac{1}{8} \lambda_s = \frac{1}{8} \frac{V_s}{f_{NF}}, \quad (6)$$

where λ_s is the shear wave wavelength; f_{NF} is the cut-off frequency, and herein is 25 Hz following He and Chen (2021); V_s is the shear wave velocity, which is determined by the minimum value of the shear wave velocity in all obtained borehole data. Following He and Chen (2021), two times of the h_{\max} is used as the horizontal mesh of the soil element. Moreover, the thickness along the longitudinal direction of the structure is taken as 18 m.

The constitutive relationship of the concrete is based on the plastic-damage model (Lee & Fenves, 1998). The mechanical parameters involved in the model are listed in Table 1, and the values of all parameters are determined according to the Code for Seismic Design of Buildings (GB 50011-2010) (Ministry of Housing and Urban-Rural Development of the People's Republic of China, 2010). Figure 10 shows the uniaxial tension and compression stress-strain and damage-strain curves of the concrete. Based on the limited obtained soil profile information and considering the efficiency of the dynamic response analyses, we use the Mohr-Coulomb constitutive model to conduct the seismic response analysis of the soil-LSUS interaction system. Existing studies have used this constitutive model to

analyze the seismic response of soil. (e.g., Tabatabaiefar & Fatahi, 2014). The value of the soil properties (i.e., shear wave velocity (V_s), unit weight (γ), cohesion (c), and friction angle (φ)) are obtained through the random field of soil properties. Due to the lack of information about the Poisson's ratio of the soil, the Poisson's ratio (ν) is approximated following Ohsaki and Iwasaki (1973):

$$\nu = 0.2 + 0.3 \sqrt{1 - \frac{1}{16} (\log_{10} G - 2)^2}, \quad (7)$$

where $G = \rho V_s^2$, representing the shear modulus of the soil, which corresponds to situations where the soil is in elastic state (i.e., small deformation level of ground shaking).

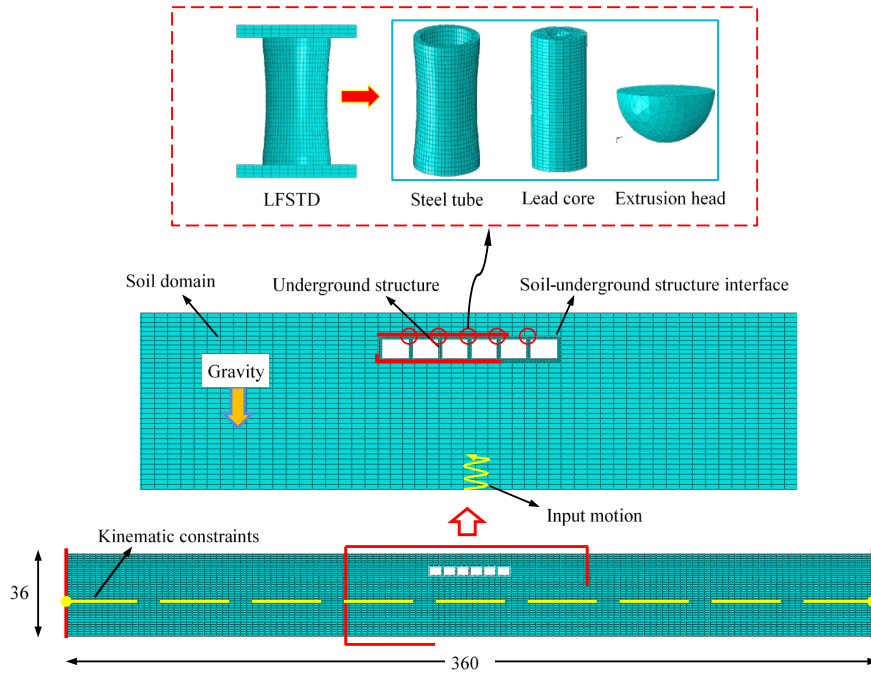


Figure 9. Numerical model layout in ABAQUS (unit: m)

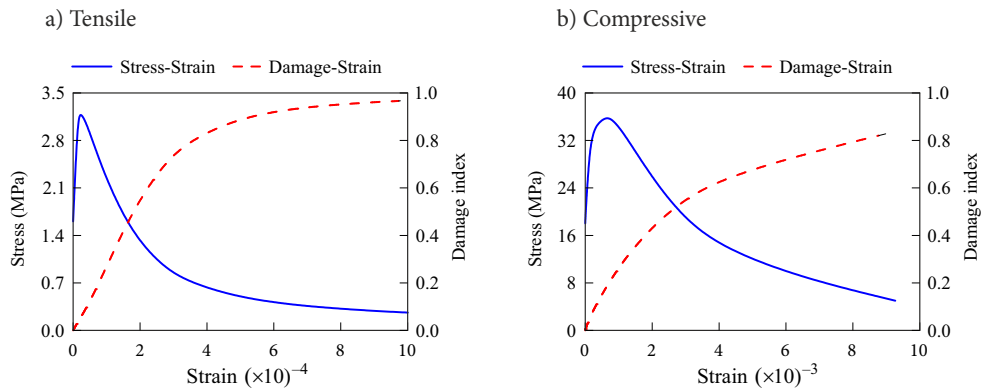


Figure 10. Characteristics of the concrete material model

Table 1. Material properties of concrete (He & Chen, 2021)

Parameters	Value	Parameters	Value
Density ρ / ($\text{kg} \cdot \text{m}^{-3}$)	2400	Limited compressive yield stress σ_{cu} / MPa	26.8
Dilation angle ψ / ($^\circ$)	30	Initial tensile yield stress σ_{t0} / MPa	2.39
Elastic modulus E / (MPa)	32500	Tensile stiffness recovery parameter ω_t	0
Poisson's ratio ν	0.2	Compressive stiffness recovery parameter ω_c	1
Initial compressive yield stress σ_{c0} / MPa	9.55		

Although we adopted the Mohr-Coulomb model in this study, while it should be noted that, during an earthquake, the soil will inevitably suffer reciprocating loads, and the hysteresis behavior of the soil could affect its dynamic response under earthquake loadings. A constitutive model that can better reflect the real behavior of soil under earthquake loadings will be used in further studies.

For the LFSTD, the solid element (C3D8R) is used for modeling, and the mesh size is taken as 10 mm. The steel adopts the bilinear constitutive model, with a yield strength of 254 MPa and ultimate strength of 554 MPa, and the post-yielding stiffness is selected as 1% of the initial stiffness. Following Lu et al. (2017), the lead is modeled by the ideal elastoplastic constitutive model, with an elastic modulus of 1.65×10^4 MPa, Poisson's ratio of 0.42, and tensile yield strength of 11 MPa. Tie constraint is adopted to combine the steel tube and the two endplates, and the contact behavior at the interface between the steel tube and lead core is simulated by hard contact. For the dimension of the LFSTD used in the analysis, the height of 300 mm, the steel tube thickness of 18 mm, and the lead core diameter of 100 mm are selected.

In the example, the shear wave velocity of the soil shows the obvious changes with depth. To this end, we model the mean field and spatial covariance in Eqn (1)

using the depth as the regressor $s(\mathbf{x})$. To consider the potential non-linear correlation between the soil properties and depth, we use a quadratic function to simulate the mean field $M(\mathbf{x})$:

$$M(\mathbf{x}) = M[s(\mathbf{x})] = \theta_{M,0} + \theta_{M,1}s(\mathbf{x}) + \theta_{M,2}s(\mathbf{x})^2, \quad (8)$$

where $[\theta_{M,0}, \theta_{M,1}, \theta_{M,2}]$ are the model parameters.

For the covariance of the zero-mean field $Z(\mathbf{x})$, the exponential function is used:

$$\text{Cov}[Z(\mathbf{x}), Z(\mathbf{x}')] = \sigma^2 \exp(\mathbf{d}_{\mathbf{xx}'} / \theta_Z). \quad (9)$$

The parameters to be determined in the random field model are estimated through the MCMC approach mentioned in Section 1. Based on the matrix decomposition approach introduced in Section 1, a total of 15 groups (i.e., R1~R15) soil property spatial random field is generated. As an example, Figure 11 shows the realization of one group (i.e., R1). The grid size used to generate the random field is the same as the mesh size of the soil element in the FE model. Then, we assign the soil properties obtained in the random field to the corresponding soil element of the FE model.

There is a clear difference between the LSUS and soil, so we use the master-slave surface contact algorithm to

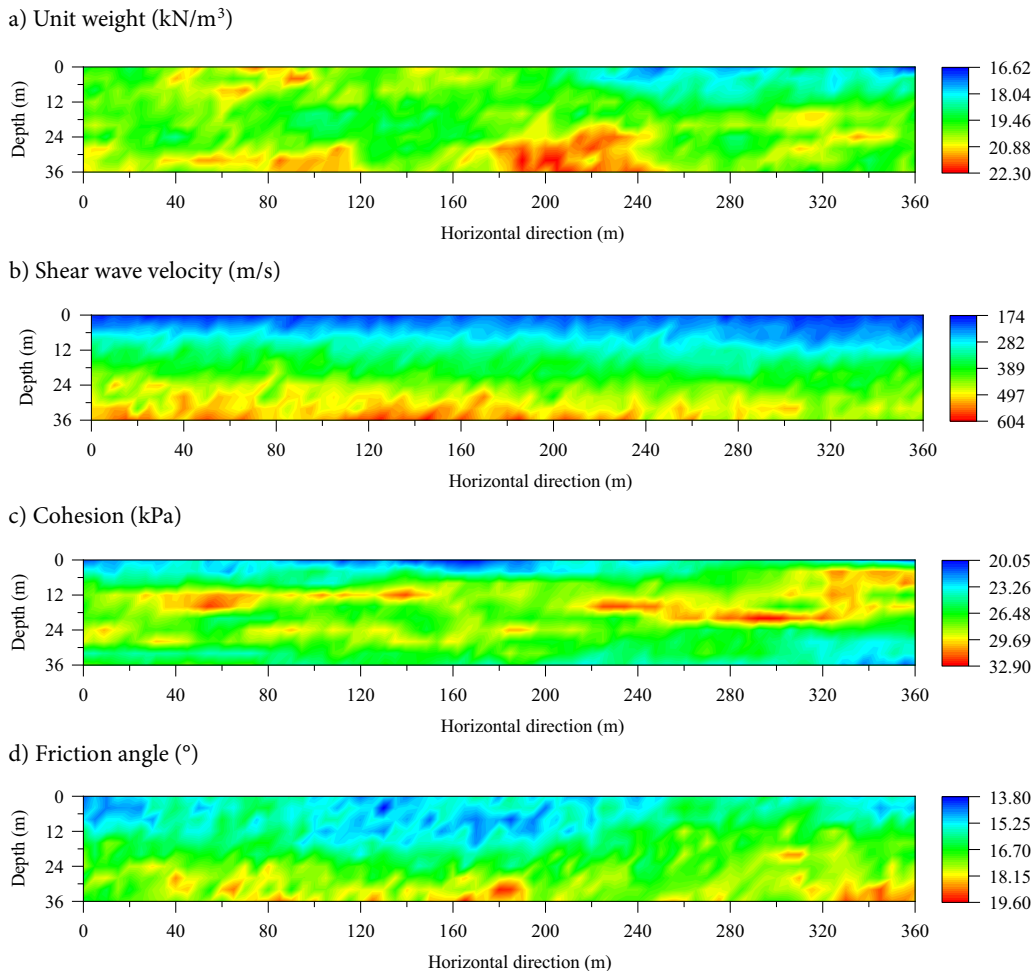


Figure 11. Realization of spatial varying soil properties

simulate the contact mechanical behavior among them. Hard contact (as shown in Figure 12a) is adopted in the normal direction of the contact. That is, when the master and slave surface are in contact, the normal force will be transferred between these two surfaces, and when the surfaces are separated, the constraint relationship will disappear and the force will no longer be transmitted between the contact surfaces. For the tangential direction of the contact, the Coulomb friction law (as shown in Figure 12b) is used, and the friction coefficient is taken as 0.4 following Zhuang et al. (2019). The inherent viscous damping of the structure and soil is described by the Rayleigh damping model, and the corresponding proportional coefficients of the damping matrix are determined by analyzing the natural vibration characteristics of the soil-LSUS interaction system. Following Castaldo et al. (2013) and Castaldo and De luliis (2014), 5% is used as an initial damping ratio for both soil and structure.

Following He and Chen (2021), the combined static-dynamic loading process is adopted in the analysis, which is shown in Figure 13. It is inevitable that the construction of LSUSs will disturb the initial stress state of the soil. To this end, it is necessary to satisfy the initial equilibrium state of the structure and soil before the dynamic analysis of the interaction system (i.e., to ensure that the soil and structure are on the stress state, and the initial displacement of the structure should be zero). Steps of applying the initial state to the soil domain are as follows: 1) constrain the degrees of freedom (DoF) in all directions at the bottom and the horizontal DoF at the lateral boundary,

2) obtain the reaction force on the lateral boundary and the stress state of all elements under the gravity loading, 3) reverse and apply the reaction force obtained from the static analysis to the lateral boundary, and the element stress state is simultaneously applied. Based on the above steps, the initial conditions of the lateral boundary for dynamic analysis can be obtained. During the dynamic analysis process, the DoF in all direction at the bottom of the model is released and the DoF in other directions are constrained. The seismic wave input through the form of acceleration, and is applied to each node at the bottom of the FE model. Figure 14 shows the seismic motion records used in this study, which recorded on the Kobe Port Island (recorded at a depth of 32 m, which is consistent with the depth of the assumed bedrock of the studied site) during the 1995 Kobe earthquake. The corresponding site (i.e., $V_{s30} = 320$ m/s) of the selected record is similar to the site (i.e., $V_{s30} = 343$ m/s) of the studied case. To balance the calculation accuracy and efficiency, a total of 25 seconds is set as the analytical duration time.

4.3. Discussion

4.3.1. Lateral deformation of the intermediate column

Figure 15a shows the time-history curves of the lateral deformation of the intermediate column under different spatial random fields of soil properties. The lateral deformation of the central column shows obvious fluctuations under different random fields of the soil. The positive and negative lateral deformation of the intermediate column

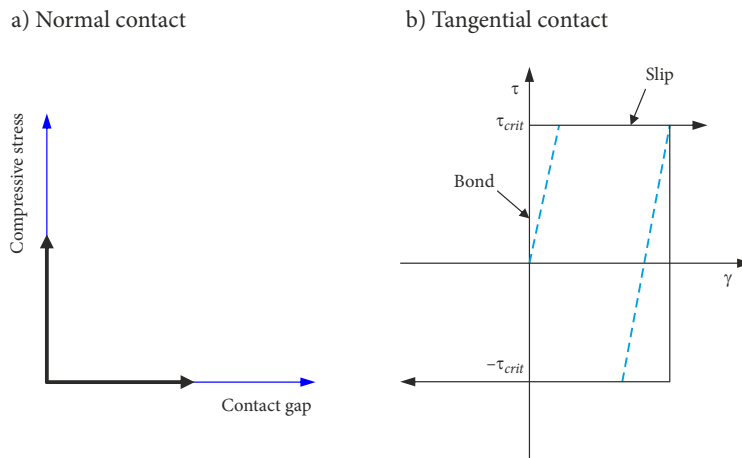


Figure 12. Contact definition between soil and underground structures

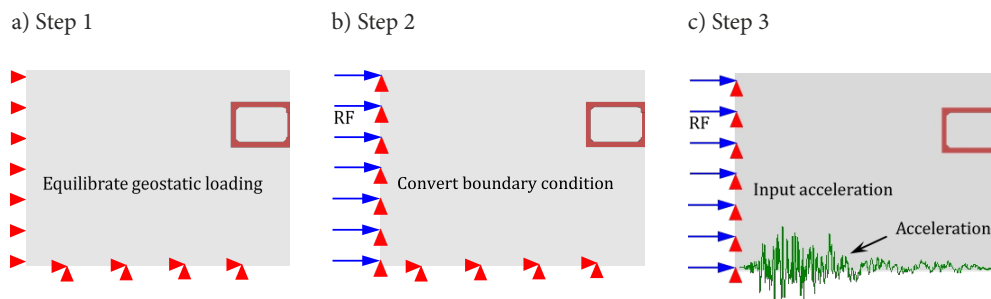


Figure 13. Boundary condition change process

is between 7.61 mm and 8.81 mm, and 7.60 mm and 8.60 mm, respectively. The maximum lateral deformation along the positive and negative direction under different spatial random fields, and the lateral deformation of the mean field are illustrated in Figure 15b. The results based on the mean-field are basically consistent with the mean of the results based on the random field. The results of multiple random response analyses can envelop the mean-field analysis results.

4.3.2. Shear force of the intermediate column

Figure 16a shows the time-history curves of the shear force of the intermediate column under different spatial random fields of soil properties. An obvious fluctuation under different random fields of the soil is also observed and with consistent the change law of the lateral deformation. The maximum positive and negative shear force is between 276.9 and 293.7 kN, and between 265.4 and

286.4 kN, respectively. Figure 16b shows the peak shear force along the positive and negative directions under different spatial random fields and the mean field. The random response results fluctuate up and down relative to the mean-field, indicating that if the seismic design of the LSUS only adopts the mean-field without considering the influence of the random field of the formation, the structural design would present a risk of insecurity.

4.3.3. Performance of LFSTDs

Figure 17 shows the hysteresis curve of the LFSTD under various spatial random field of soil properties. Two obvious differences could be observed, one is the difference between the positive and negative deformation of the LFSTD, and the other is the difference in the path of the hysteresis loop. It is worth mentioning that in cases R4, R5, R7, R8, R9, R10, R11, R13, and R14, the peak deformation of the LFSTD has exceeded the ultimate deformation (i.e., 20 mm),

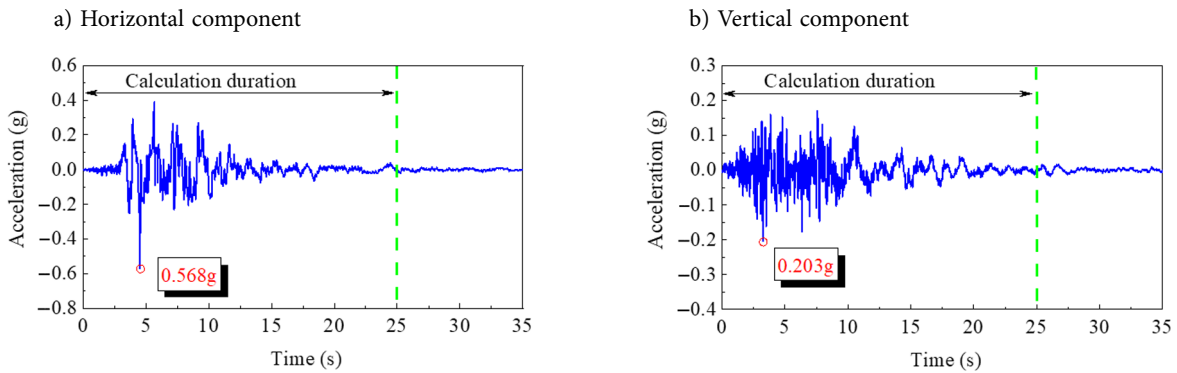


Figure 14. Earthquake recordings at the Kobe Port Island (Nguyen et al., 2020)

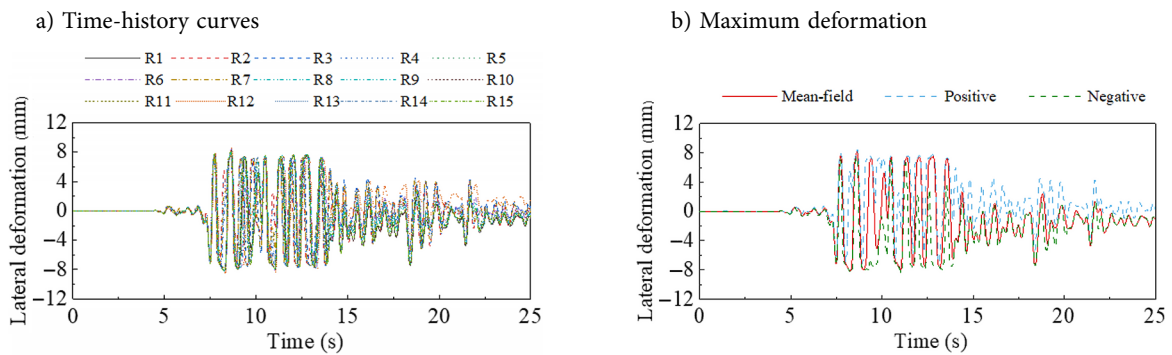


Figure 15. Lateral deformation of the intermediate column

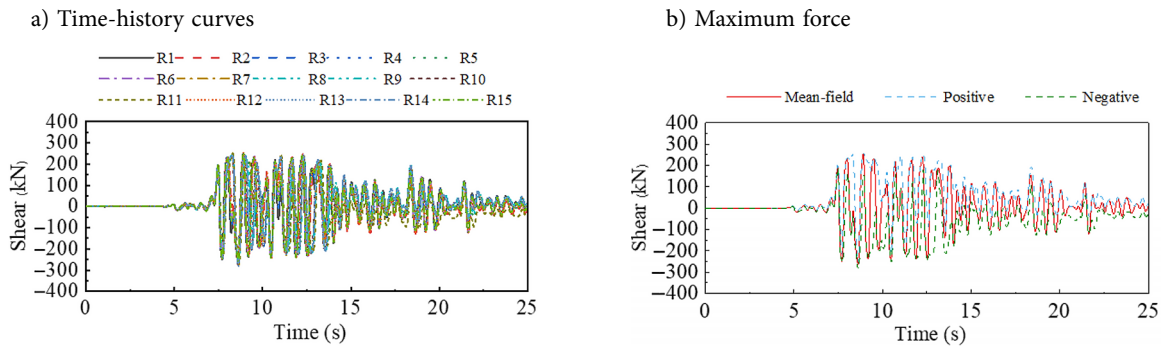


Figure 16. Shear force of the central column

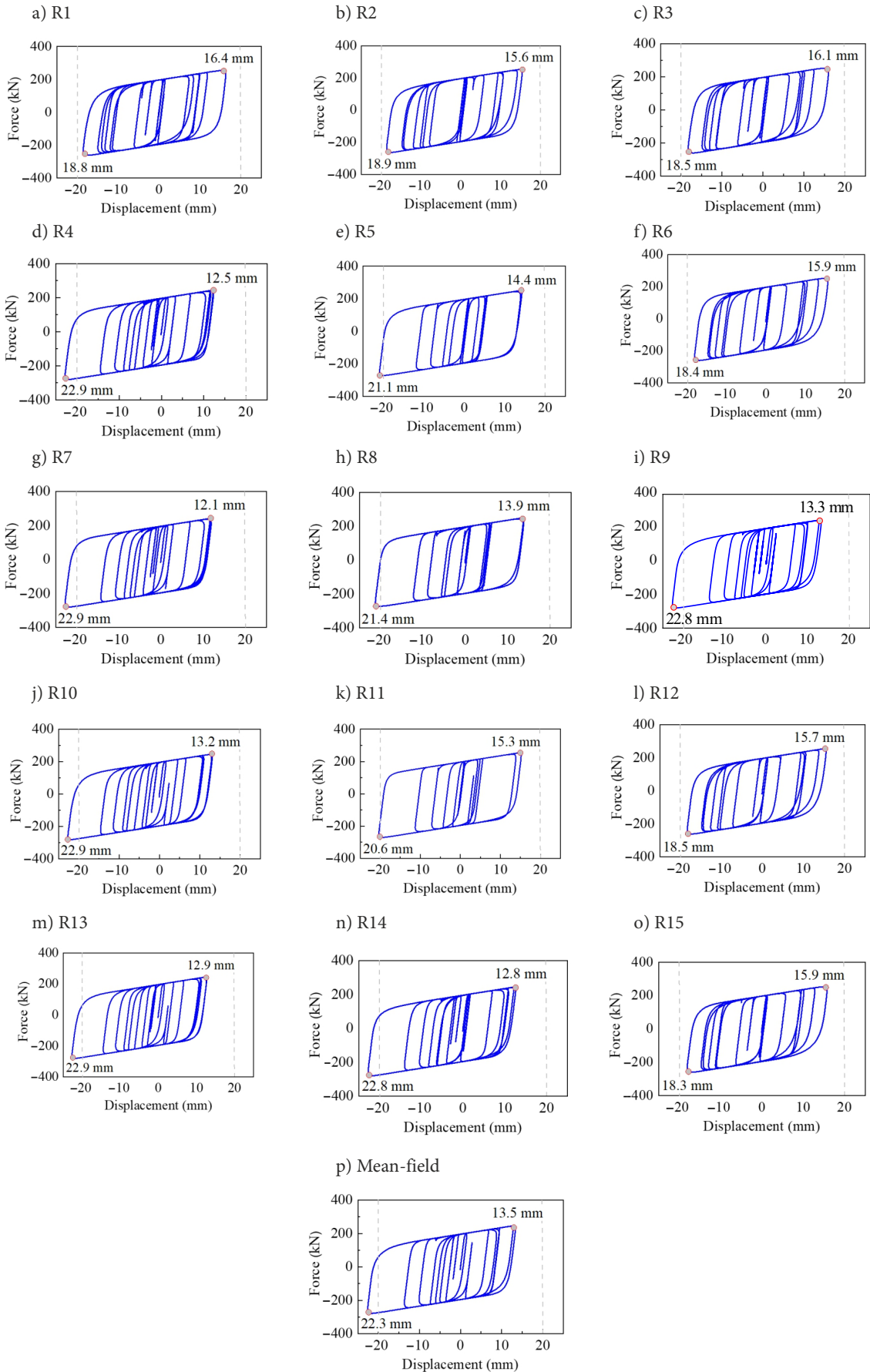


Figure 17. Hysteresis curve of the LFSTD

which means the LFSTD will suffer failure. The peak deformation of the LFSTD is between 12.1 and 16.4 mm (i.e., along the positive direction), and between 18.3 and 22.9 mm (i.e., along the negative direction). The peak difference ratio of the positive and negative deformations of the LFSTDs of all cases is 30.2% and 22.3%. The peak deformation of the LFSTD under the mean-field is 13.5 mm (i.e., along the positive direction), and 22.3 mm (i.e., along the negative direction).

4.3.4. Energy dissipation of the structure and LFSTD

The time-history curves of energy dissipation of the LFSTD and structure are shown in Figures 18a and 18b, and the

peak energy dissipation of the LFSTD and structure are shown in Figures 19a and 19b. Whether for the LFSTD or LSUS, the peak energy dissipation shows obvious fluctuations. The maximum energy dissipation of the LFSTD is between 31.1 and 56.5 kJ, with a maximum difference ratio of 44.9%, while the peak energy dissipation of the LSUS is between 362.8 and 917.4 kJ, with a maximum difference ratio of 60.4%. Table 2 lists the ratio of the energy dissipation between the LFSTD and LSUS, and the range is between 6.2% to 8.6%, indicating that the spatially varying soil properties cause minor difference in energy dissipation ratio.

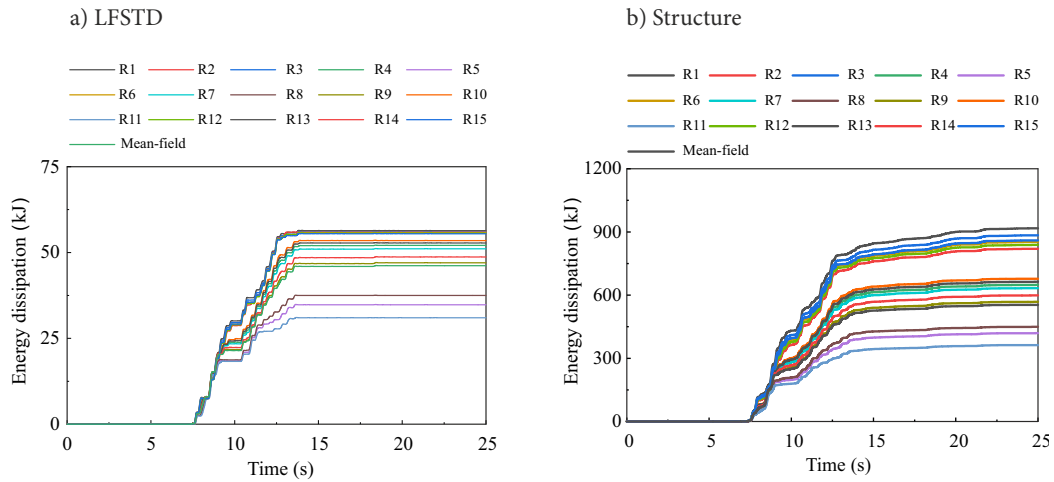


Figure 18. Time-history curves of energy dissipation

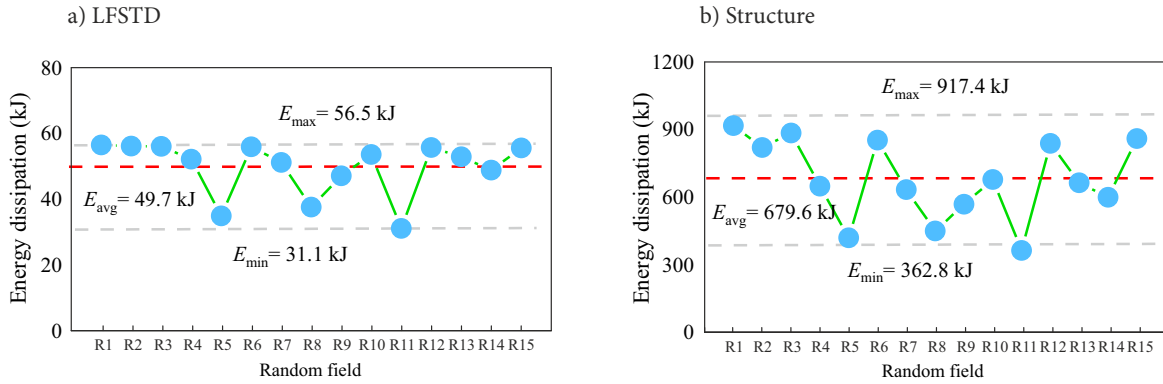


Figure 19. Peak energy dissipation

Table 2. Ratio of the energy dissipation between the LFSTD and LSUS

	Random field							
	R1	R2	R3	R4	R5	R6	R7	R8
E_{LFSTD} (kJ)	56.5	56.1	56.0	52.2	34.9	55.9	51.2	37.6
E_{LSUS} (kJ)	917.4	819.9	884.1	648.5	419.3	852.8	633.0	449.4
e (%)	6.2	6.8	6.3	8.0	8.3	6.6	8.1	8.4
	Random field							
	R9	R10	R11	R12	R13	R14	R15	Mean-field
E_{LFSTD} (kJ)	47.1	53.6	31.1	55.7	52.9	48.8	55.6	45.7
E_{LSUS} (kJ)	568.1	677.8	362.8	838.5	663.3	598.8	860.0	586.8
e (%)	8.3	7.9	8.6	6.6	8.0	8.2	6.5	7.8

The obtained results above do not show obvious rules, and this mainly attributed to that the spatial random field of different soil properties will have a certain influence on the propagation of seismic waves, which is a very complex process. Therefore, the coupling effect of the spatial variability of ground motions and the spatial variability of soil physical properties should be further studied.

5. Conclusions

This paper applying an improved latent space approach to simulate the spatially distribution of soil properties, considering the non-stationary characteristic of the spatial random field. A seismic response analysis process of the soil-large-space underground structure (LSUS) interaction system considering the spatial random distribution of soil properties is proposed. The influence of the spatial variability of soil properties on the seismic reduction effect of the LSUS is studied. Main conclusions are summarized as follows:

1. The proposed seismic response analysis process can be used in the seismic response analysis of the soil-LSUS interaction system for the situation considering the spatial variability of soil properties.
2. The spatial variability of the soil properties will have a minor influence on the force and deformation of the intermediate column and the energy dissipation ratio between the LFSTD and structure, while will cause a significant impact on the maximum deformation, maximum force, energy dissipation, and the shape and path of the hysteresis loop.
3. For the seismic mitigation design of LSUSs, the influence of the spatial variability of the soil properties can be ignored provided only the performance of the structure (such as the deformation and force of the intermediate column) are concerned. While it is necessary to consider the spatial variability of the soil properties if it is necessary to accurately obtain the performance of the LFSTD.

Conflict of interest

The authors have no conflicts of interest to declare.

Acknowledgements

The authors would like to acknowledge the financial support from the National Natural Science Foundation of China (Grant no. 51778489), the China Scholarship Council (Grant No. 201806260175), and the National Key Research and Development Program of China (No. 2017YFC0703600). The authors also would like to express their sincere gratitude to the editor and the anonymous reviewers who significantly enhanced the contents of the study with their insightful comments.

References

- Box, G. E., & Cox, D. R. (1964). An analysis of transformations. *Journal of the Royal Statistical Society: Series B (Methodological)*, 26, 211–243. <https://doi.org/10.1111/j.2517-6161.1964.tb00553.x>
- Castaldo, P., Calvello, M., & Palazzo, B. (2013). Probabilistic analysis of excavation-induced damages to existing structures. *Computers and Geotechnics*, 53, 17–30. <https://doi.org/10.1016/j.compgeo.2013.04.008>
- Castaldo, P., & De Luliis, M. (2014). Effects of deep excavation on seismic vulnerability of existing reinforced concrete framed structures. *Soil Dynamics and Earthquake Engineering*, 64, 102–112. <https://doi.org/10.1016/j.soildyn.2014.05.005>
- Chen, Z.-Y., Chen, W., & Bian, G.-Q. (2014). Seismic performance upgrading for underground structures by introducing shear panel dampers. *Advances in Structural Engineering*, 17, 1343–1357. <https://doi.org/10.1260/1369-4332.17.9.1343>
- Davis, M. W. (1987). Production of conditional simulations via the LU triangular decomposition of the covariance matrix. *Mathematical Geology*, 19, 91–98. <https://doi.org/10.1007/BF00898189>
- Deodatis, G. (1996). Simulation of ergodic multivariate stochastic processes. *Journal of Engineering Mechanics*, 122, 778–787. [https://doi.org/10.1061/\(ASCE\)0733-9399\(1996\)122:8\(778\)](https://doi.org/10.1061/(ASCE)0733-9399(1996)122:8(778))
- Ding, J.-H., Jin, X.-L., Guo, Y.-Z., & Li, G.-G. (2006). Numerical simulation for large-scale seismic response analysis of immersed tunnel. *Engineering Structures*, 28, 1367–1377. <https://doi.org/10.1016/j.engstruct.2006.01.005>
- Do, N.-A., Dias, D., Oreste, P., & Djeran-Maigre, I. (2015). 2D numerical investigation of segmental tunnel lining under seismic loading. *Soil Dynamics and Earthquake Engineering*, 72, 66–76. <https://doi.org/10.1016/j.soildyn.2015.01.015>
- European Committee for Standardization. (2005). *Eurocode 8: Design of structures for earthquake resistance. Part 1: General rules, seismic actions and rules for buildings* (EN 1998-1). Brussels.
- Federal Emergency Management Agency. (2000). *Prestandard and commentary for the seismic rehabilitation of buildings* (FEMA 356). Washington DC.
- Haldar, S., & Babu, G. S. (2008). Effect of soil spatial variability on the response of laterally loaded pile in undrained clay. *Computers and Geotechnics*, 35, 537–547. <https://doi.org/10.1016/j.compgeo.2007.10.004>
- Hariri-Ardebili, M. A., Seyed-Kolbadi, S. M., Saouma, V. E., Salamoun, J. W., & Nuss, L. K. (2019). Anatomy of the vibration characteristics in old arch dams by random field theory. *Engineering Structures*, 179, 460–475. <https://doi.org/10.1016/j.engstruct.2018.10.082>
- He, Z., & Chen, Q. (2021). Upgrading the seismic performance of underground structures by introducing lead-filled steel tube dampers. *Tunnelling and Underground Space Technology*, 108, Article 103727. <https://doi.org/10.1016/j.tust.2020.103727>
- He, Z., Xu, H., Gardoni, P., Zhou, Y., Wang, Y., & Zhao, Z. (2022). Seismic demand and capacity models, and fragility estimates for underground structures considering spatially varying soil properties. *Tunnelling and Underground Space Technology*, 119, Article 104231. <https://doi.org/10.1016/j.tust.2021.104231>
- Huang, H., Gong, W., Khoshnevisan, S., Juang, C. H., Zhang, D., & Wang, L. (2015). Simplified procedure for finite element analysis of the longitudinal performance of shield tunnels considering spatial soil variability in longitudinal direction. *Computers and Geotechnics*, 64, 132–145. <https://doi.org/10.1016/j.compgeo.2014.11.010>

- Huang, X., Zhou, X., Ma, W., Niu, Y., & Wang, Y. (2017). Two-dimensional stability assessment of rock slopes based on random field. *International Journal of Geomechanics*, 17, Article 04016155. [https://doi.org/10.1061/\(ASCE\)GM.1943-5622.0000858](https://doi.org/10.1061/(ASCE)GM.1943-5622.0000858)
- Kim, H.-K., & Santamarina, J. C. (2008). Spatial variability: drained and undrained deviatoric load response. *Geotechnique*, 58, 805–814. <https://doi.org/10.1680/geot.2008.3724>
- Kim, H., & Shields, M. D. (2015). Modeling strongly non-Gaussian non-stationary stochastic processes using the iterative translation approximation method and Karhunen–Loève expansion. *Computers & Structures*, 161, 31–42. <https://doi.org/10.1016/j.compstruc.2015.08.010>
- Lee, J., & Fenves, G. L. (1998). Plastic-damage model for cyclic loading of concrete structures. *Journal of Engineering Mechanics*, 124, 892–900. [https://doi.org/10.1061/\(ASCE\)0733-9399\(1998\)124:8\(892\)](https://doi.org/10.1061/(ASCE)0733-9399(1998)124:8(892))
- Lizarraga, H. S., & Lai, C. G. (2014). Effects of spatial variability of soil properties on the seismic response of an embankment dam. *Soil Dynamics and Earthquake Engineering*, 64, 113–128. <https://doi.org/10.1016/j.soildyn.2014.03.016>
- Lu, D., Zhou, Y., Deng, X., & Zhang, C. (2017). Optimization of configuration and finite element modeling for lead-filled steel tube dampers. *Engineering Mechanics*, 34(3), 76–83 (in Chinese).
- Lysmer, J., & Kuhlemeyer R. L. (1969). Finite dynamic model for infinite media. *Journal of the Engineering Mechanics Division*, 95, 859–878. <https://doi.org/10.1061/JMCEA3.0001144>
- Ma, C., Lu, D., & Du, X. (2018). Seismic performance upgrading for underground structures by introducing sliding isolation bearings. *Tunnelling and Underground Space Technology*, 74, 1–9. <https://doi.org/10.1016/j.tust.2018.01.007>
- Ministry of Housing and Urban-Rural Development of the People's Republic of China. (2010). *Code for seismic design of buildings* (GB 50011-2010). Beijing: China Architecture & Building Press.
- Na, U. J., Chaudhuri, S. R., & Shinozuka, M. (2009). Effects of spatial variation of soil properties on seismic performance of port structures. *Soil Dynamics and Earthquake Engineering*, 29, 537–545. <https://doi.org/10.1016/j.soildyn.2008.06.002>
- National Standardization Management Committee. (2005). *Evaluation of seismic safety for engineering sites* (GB 17741-2005). China Standard Press.
- Nguyen, V.-Q., Nizamani, Z. A., Park, D., & Kwon, O.-S. (2020). Numerical simulation of damage evolution of Daikai station during the 1995 Kobe earthquake. *Engineering Structures*, 206, Article 110180. <https://doi.org/10.1016/j.engstruct.2020.110180>
- Ohzaki, Y., & Iwasaki, R. (1973). On dynamic shear moduli and Poisson's ratios of soil deposits. *Soils and Foundations*, 13, 61–73. https://doi.org/10.3208/sandf1972.13.4_61
- Papaioannou, I., & Straub, D. (2012). Reliability updating in geotechnical engineering including spatial variability of soil. *Computers and Geotechnics*, 42, 44–51. <https://doi.org/10.1016/j.compgeo.2011.12.004>
- Popescu, R. (1995). *Stochastic variability of soil properties: data analysis, digital simulation, effects on system behavior*. Princeton University, New Jersey.
- Popescu, R., Deodatis, G., & Nobahar, A. (2005). Effects of random heterogeneity of soil properties on bearing capacity. *Probabilistic Engineering Mechanics*, 20, 324–341. <https://doi.org/10.1016/j.probengmech.2005.06.003>
- Tabatabaiefar, H. R., & Fatahi, B. (2014). Idealisation of soil–structure system to determine inelastic seismic response of mid-rise building frames. *Soil Dynamics and Earthquake Engineering*, 66, 339–351. <https://doi.org/10.1016/j.soildyn.2014.08.007>
- Tsinidis, G., de Silva, F., Anastasopoulos, I., Bilotta, E., Bobet, A., Hashash, Y. M., He, C., Kampas, G., Knappett, J., Madabhushi, G., Nikitas, K., Silvestri, F., Viggiani, G., & Fuentes, R. (2020). Seismic behaviour of tunnels: From experiments to analysis. *Tunnelling and Underground Space Technology*, 99, Article 103334. <https://doi.org/10.1016/j.tust.2020.103334>
- VanMarcke, E. (1983). *Random fields: analysis and synthesis*. Rare Book Services, Princeton University, Princeton NJ.
- Wang, H.-f., Lou, M.-l., & Zhang, R.-l. (2017). Influence of presence of adjacent surface structure on seismic response of underground structure. *Soil Dynamics and Earthquake Engineering*, 100, 131–143. <https://doi.org/10.1016/j.soildyn.2017.05.031>
- Wang, Y., Cao, Z., & Au, S.-K. (2011). Practical reliability analysis of slope stability by advanced Monte Carlo simulations in a spreadsheet. *Canadian Geotechnical Journal*, 48, 162–172. <https://doi.org/10.1139/T10-044>
- Wang, Y., Chen, Q., Zhao, Z., & He, Z. (2021). A resilient column with angular friction damper for seismic performance upgrading of underground structures. *Tunnelling and Underground Space Technology*, 116, Article 104085. <https://doi.org/10.1016/j.tust.2021.104085>
- Xu, H., & Gardoni, P. (2018). Improved latent space approach for modelling non-stationary spatial-temporal random fields. *Spatial Statistics*, 23, 160–181. <https://doi.org/10.1016/j.jspasta.2018.01.003>
- Xu, H., & Gardoni, P. (2020). Conditional formulation for the calibration of multi-level random fields with incomplete data. *Reliability Engineering & System Safety*, 204, Article 107121. <https://doi.org/10.1016/j.res.2020.107121>
- Yamato, T., Umehara, T., Aoki, H., Nakamura, S., Ezaki, J., & Suetomi, I. (1996). Damage to Daikai subway station of kobe rapid transit system and estimation of its reason during the 1995 Hyogoken-Nanbu earthquake. In *Earthquake geotechnical case histories for performance-based design* (pp. 303–320). Routledge. https://doi.org/10.2208/jscej.1996.537_303
- Yu, H., Yuan, Y., Qiao, Z., Gu, Y., Yang, Z., & Li, X. (2013). Seismic analysis of a long tunnel based on multi-scale method. *Engineering Structures*, 49, 572–587. <https://doi.org/10.1016/j.engstruct.2012.12.021>
- Yu, H., Xiao, W., Yuan, Y., & Taerwe, L. (2017). Seismic mitigation for immersion joints: Design and validation. *Tunnelling and Underground Space Technology*, 67, 39–51. <https://doi.org/10.1016/j.tust.2017.04.018>
- Zhang, L., & Liu, Y. (2020). Numerical investigations on the seismic response of a subway tunnel embedded in spatially random clays. *Underground Space*, 5(1), 43–52. <https://doi.org/10.1016/j.undsp.2018.10.001>
- Zhuang, H., Ren, J., Miao, Y., Jing, L., Yao, E., & Xu, C. (2019). Seismic performance levels of a large underground subway station in different soil foundations. *Journal of Earthquake Engineering*, 25(4), 2808–2833. <https://doi.org/10.1080/13632469.2019.1651423>